Electronic Supplementary Information

Highly Efficient Blue-Green Dual-Narrow-Emission in $RbAl_{11}O_{17}:Eu^{2+}$, Mn^{2+} toward Wide-Color-Gamut Human-Centric Backlights

Yali Xue, Yujun Liang*, Weilun Zhang, Xiaodeng Wu, Chuang Han

Engineering Research Center of Nano-Geomaterials of Ministry of Education, Faculty of Materials Science and Chemistry, China University of Geosciences, Wuhan 430074, China. E-mail: yujunliang@sohu.com

Table S1. Photoluminescence properties of several green-emitting phosphors for backlight display applications.

Phosphors	λ_{em} (nm)	FWHM (nm)	λ_{ex} (nm)	Thermal behavior	IQE	NTSC	Ref.
β-sialon:Eu^{2+}	540	55	405	81% (150 °C)	71%	101%	13
γ-AlON:Mn^{2+}	520	44	445	76% (150 °C)	62%	102%	25
$LaZnAl_{11}O_{19}$:Eu^{2+}, Mn^{2+}	515	26	350	80% (150 °C)	88%	123%	23
$MgAl_2O_4$:Mn^{2+}	525	35	450	92% (150 °C)	45%	116%	26
$Sr_2MgAl_{22}O_{36}$:Mn^{2+}	518	26	450	80% (150 °C)	75%	127%	27
$BaZnAl_{10}O_{17}$:Mn^{2+}	516	31	450	88% (150 °C)	86%	110%	28
$CsPbBr_3$	523	20	450	62% (150 °C)	63%	102%	55
$RbAl_{11}O_{17}$:Eu^{2+}, Mn^{2+}	511	26	345	54% (150 °C)	63%	118%	This work

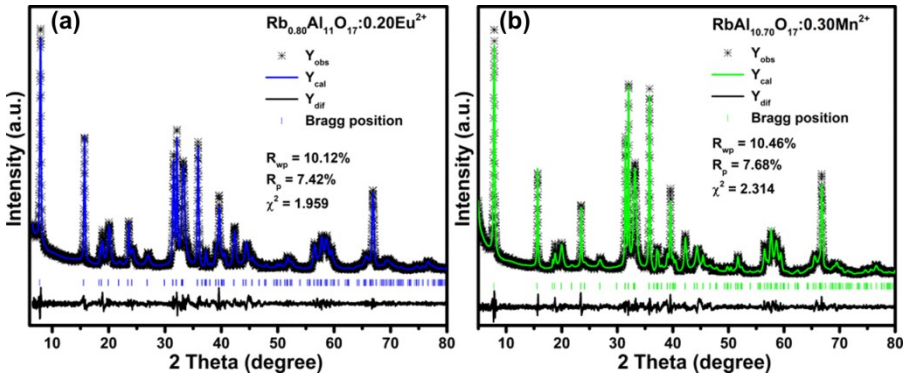

Figure S1 Rietveld refinement patterns of $Rb_{0.80}Al_{11}O_{17}$:0.20Eu^{2+} and $RbAl_{10.70}O_{17}$:0.30Mn^{2+} samples.

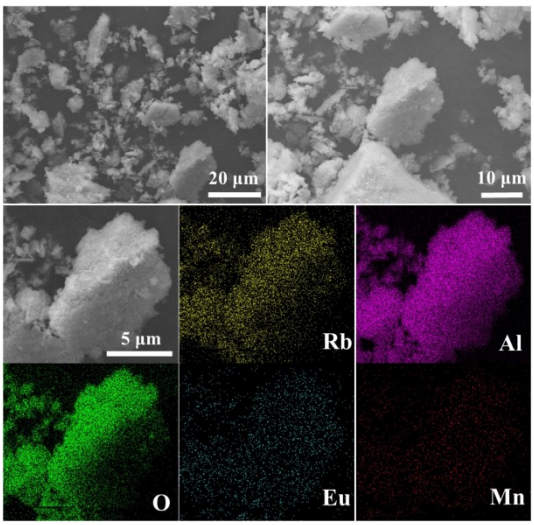

Figure S2 The morphology and elemental distribution of $Rb_{0.80}Al_{10.95}O_{17}$:0.20$Eu^{2+}$, 0.05$Mn^{2+}$.

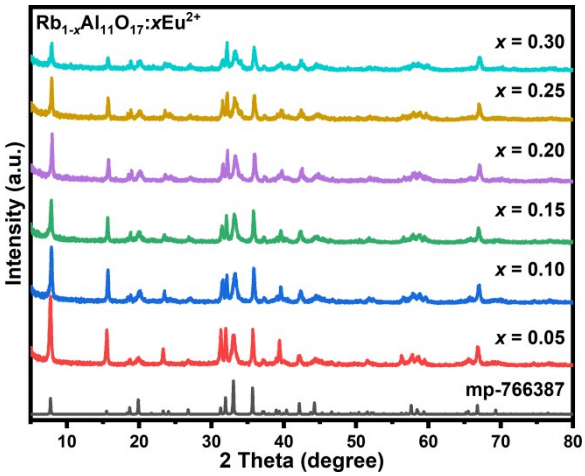

Figure S3 XRD patterns of $Rb_{1-x}Al_{11}O_{17}$:xEu^{2+} with the standard $RbAl_{11}O_{17}$ data.

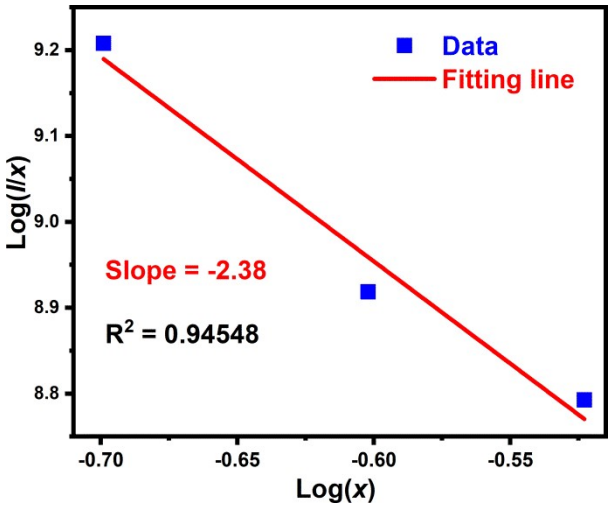

Figure S4 The relationship between lg(I/x) and lg(x) in $Rb_{1-x}Al_{11}O_{17}$:xEu^{2+}.

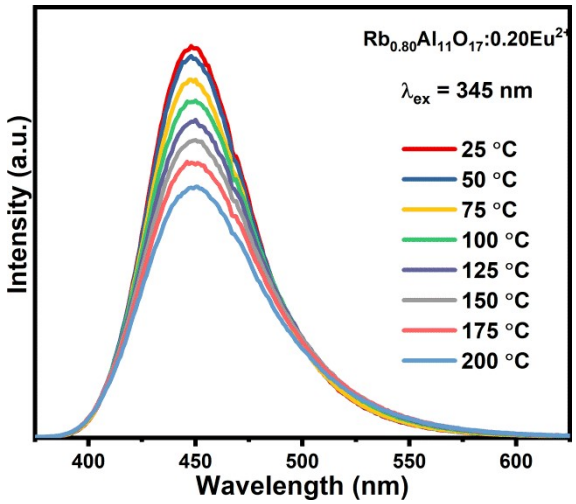

Figure S5 Temperature-dependent emission spectra of $Rb_{0.80}Al_{11}O_{17}:0.20Eu^{2+}$.

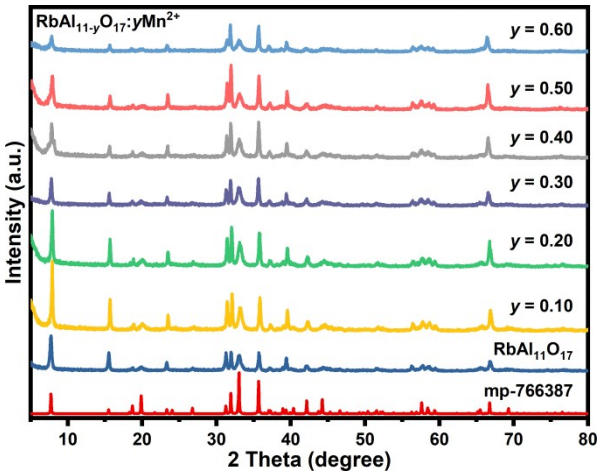

Figure S6 XRD patterns of $RbAl_{11-y}O_{17}$:yMn^{2+} with the standard data.

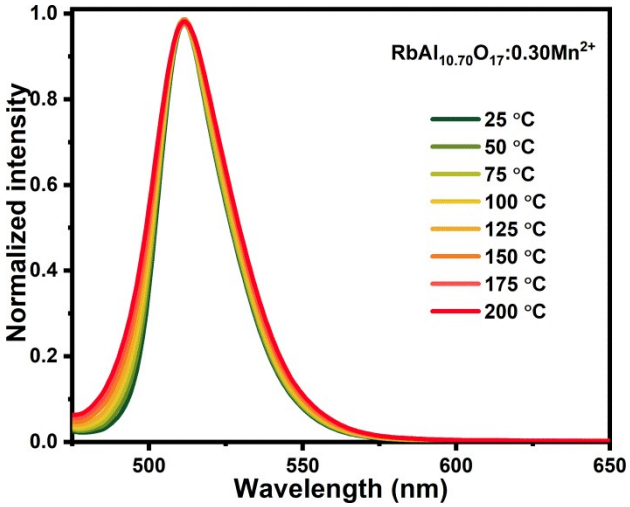

Figure S7 The normalized emission spectra of $RbAl_{10.70}O_{17}:0.30Mn^{2+}$ at different temperatures.

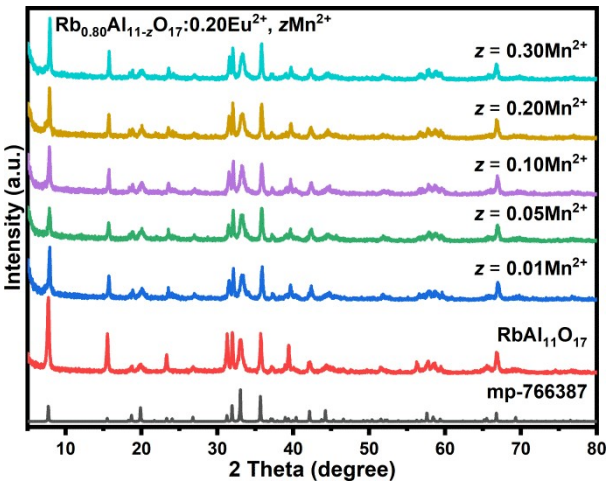

Figure S8 XRD patterns of $Rb_{0.80}Al_{11-z}O_{17}$:0.20Eu^{2+}, zMn^{2+} with the standard data.

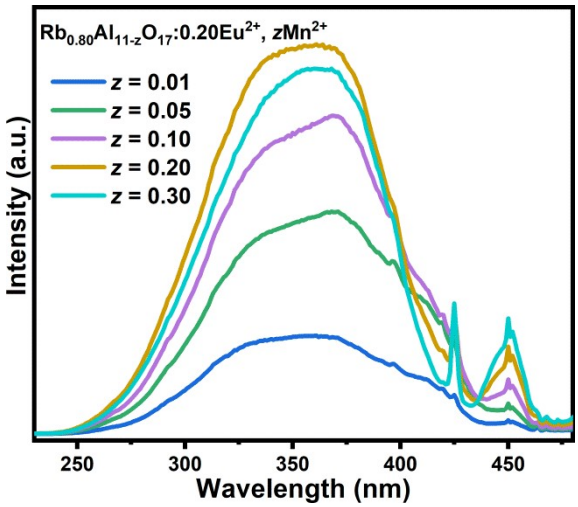

Figure S9 The excitation spectra of $Rb_{0.80}Al_{11-z}O_{17}$:0.20Eu^{2+}, $z$$Mn^{2+}$ with 510 nm emission.

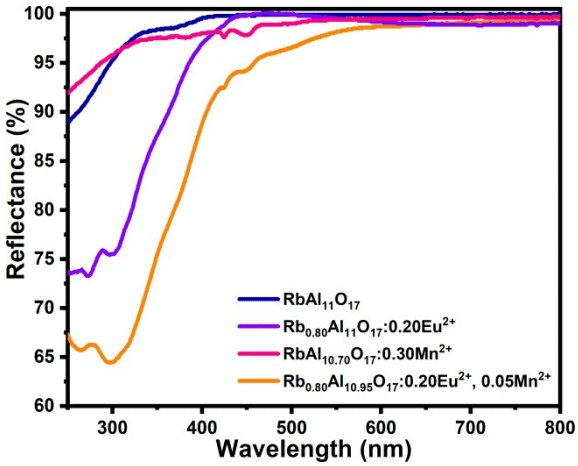

Figure S10 UV-vis diffuse reflectance spectra of the $RbAl_{11}O_{17}$, $Rb_{0.80}Al_{11}O_{17}$:0.20Eu^{2+}, $RbAl_{10.70}O_{17}$:0.30Mn^{2+} and $Rb_{0.80}Al_{10.95}O_{17}$:0.20$Eu^{2+}$, 0.05$Mn^{2+}$ samples.

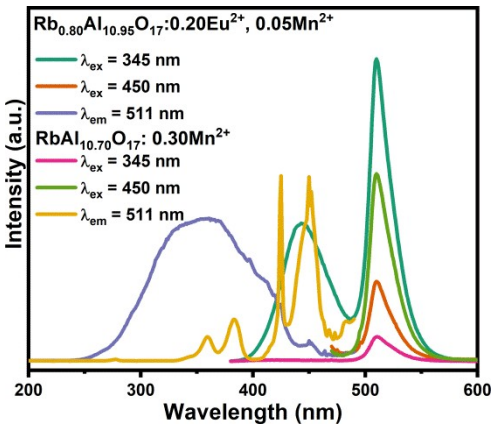

Figure S11 Emission (λ_{ex} = 345, 450 nm) and excitation (λ_{em} = 511 nm) spectra of $Rb_{0.80}Al_{10.95}O_{17}$:0.20$Eu^{2+}$, 0.05$Mn^{2+}$ and $RbAl_{10.70}O_{17}$:0.30Mn^{2+}.

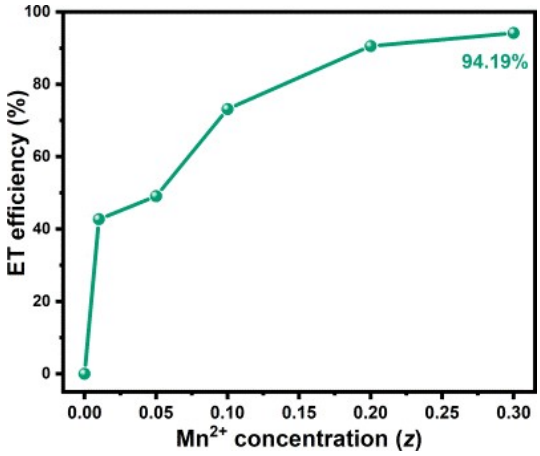

Figure S12 The η_{ET} depending on the Mn^{2+} doping concentration in $Rb_{0.80}Al_{11-z}O_{17}$:0.20Eu^{2+}, $z$$Mn^{2+}$ phosphors.

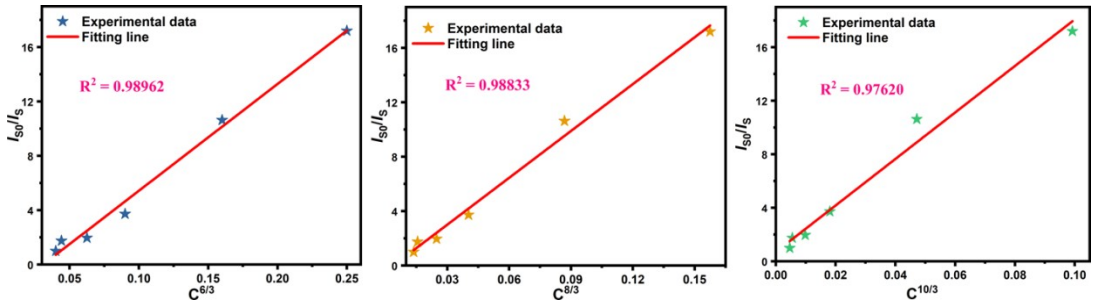

Figure S13 Linear fits of I_0/I_S and $C^{n/3}$ at n values of 6, 8 and 10 in $Rb_{0.80}Al_{10.80}O_{17}$:0.20$Eu^{2+}$, 0.2$Mn^{2+}$.

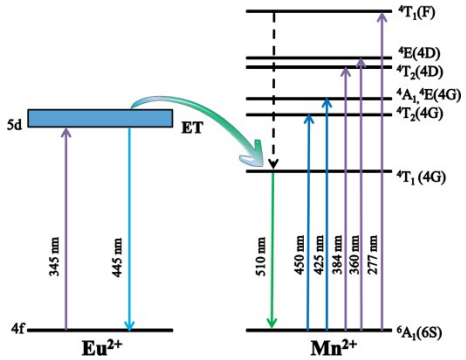

Figure S14 The energy transfer process between Eu^{2+} and Mn^{2+} in $RbAl_{11}O_{17}$:Eu^{2+}, Mn^{2+}.

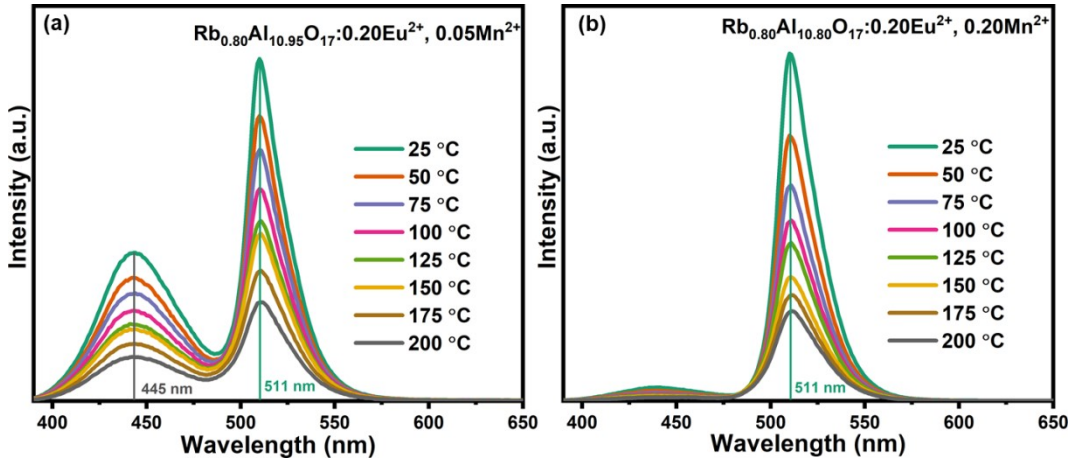

Figure S15 Temperature-dependent emission intensity of $R_{0.80}A_{10.95}O$:0.20Eu^{2+}, 0.05Mn^{2+} and $R_{0.80}A_{10.80}O$:0.20Eu^{2+}, 0.20Mn^{2+} during the heating process under a 345 nm UV light source.

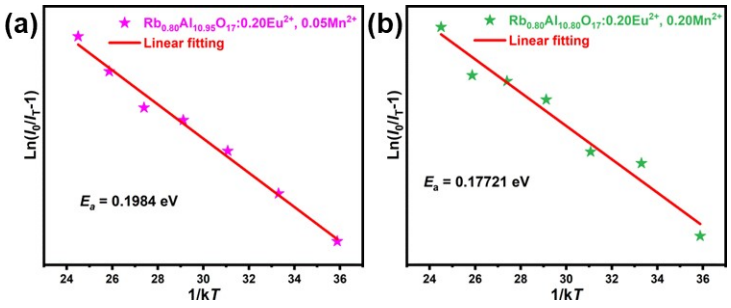

Figure S16 The activation energy (Ea) of $Rb_{0.80}Al_{10.95}O_{17}$:0.20$Eu^{2+}$, 0.05$Mn^{2+}$ and $Rb_{0.80}Al_{10.80}O_{17}$:0.20$Eu^{2+}$, 0.20$Mn^{2+}$.